EXPERIMENTAL PROGRESS TOWARD DETECTION AND IDENTIFICATION OF ELECTROMAGNETICALLY COMPLEX STRUCTURES

S.A. von Laven and N.G. Albritton
H. M. Jaenisch and J. W. Handley
Amtec Corporation
Huntsville, Alabama 35816-3429

T.A. Baginski and A.S. Hodel
Auburn University
Auburn, Alabama 36849-5201

R.W. McMillan
U.S. Army Space & Missile Defense Command
Huntsville, Alabama 35807-3801

I. Kohlberg
Kohlberg Associates
Reston, Virginia 20190-4440

ABSTRACT

Radio frequency (RF) signatures have been observed in the scattered return when a passive electromagnetically complex target structure is excited with a broadband pulse. The target range can be reliably determined up to a maximum range that is subject to equipment limitations. The range dependence of the return is found to be consistent with theoretical predictions, which include the role played by soil conductivity.

1. INTRODUCTION

Many activities, military and civilian, can benefit from remote detection and identification of visually obscured structures. RF detection techniques benefit from (1) RF's ability to penetrate obstacles, including soil, (2) RF's broad solid-angle coverage, (3) scalability with transmitter power, and (4) the overall maturity of RF technology.

Advances in electromagnetic detection near the ground-air interface have occurred on many fronts. These include military and homeland-defense applications (Nag and Peters, 1998; Baum, 1997; Venkatasubramanian et. al., 2004). Utilities and the construction industry also have a strong interest in such detection (Kind et. al., 2003). The agricultural research community has made contributions in the related pursuit of improved soil moisture measurements (Galagedara et. al., 2005).

Structures of interest often lie near the surface of the earth. Thus we must account for the RF properties of the ground-air interface in our detection/identification scheme. Standard simplifications often implemented when analyzing RF interactions (such as free-space propagation and far-field approximations), will not apply, in general (Hanson and Baum, 1998). We are developing the capability to use RF response to detect and identify electromagnetically complex structures near the air-earth interface. Our companion paper in the conference (Kohlberg et. al., 2008) discusses the theoretical foundations for this effort.

In Section 2 we explain our approach. In Sections 3 and 4 we describe our measurements and their interpretation. In Section 5 we present computational modeling performed with NEC. Finally, we analyze our results and summarize.

2. TECHNICAL APPROACH

A detection system with low average radiated power is desirable for most applications. Precise range measurements are desirable for applications requiring geolocation. These requirements led us to our choice of a pulsed ultra wide band (UWB) detection system.

Structures of interest (targets) have complex RF poles whose real and imaginary parts may be used to help classify them. The target response, particularly for the dominant poles, can provide a good measure of its range. We also expect that targets near the ground-air interface will have different values for their model parameters at different RF frequencies (i.e. some variables will be a

Report Documentation Page

Form Approved
OMB No. 0704-0188

1. REPORT DATE	2. REPORT TYPE	3. DATES COVERED
01 DEC 2008	**N/A**	**-**

4. TITLE AND SUBTITLE	5a. CONTRACT NUMBER
Experimental Progress Toward Detection And Identification Of Electromagnetically Complex Structures	5b. GRANT NUMBER
	5c. PROGRAM ELEMENT NUMBER
6. AUTHOR(S)	5d. PROJECT NUMBER
	5e. TASK NUMBER
	5f. WORK UNIT NUMBER
7. PERFORMING ORGANIZATION NAME(S) AND ADDRESS(ES) **Amtec Corporation Huntsville, Alabama 35816-3429**	8. PERFORMING ORGANIZATION REPORT NUMBER
9. SPONSORING/MONITORING AGENCY NAME(S) AND ADDRESS(ES)	10. SPONSOR/MONITOR'S ACRONYM(S)
	11. SPONSOR/MONITOR'S REPORT NUMBER(S)

12. DISTRIBUTION/AVAILABILITY STATEMENT
Approved for public release, distribution unlimited

13. SUPPLEMENTARY NOTES
See also ADM002187. Proceedings of the Army Science Conference (26th) Held in Orlando, Florida on 1-4 December 2008, The original document contains color images.

14. ABSTRACT

15. SUBJECT TERMS

16. SECURITY CLASSIFICATION OF:			17. LIMITATION OF ABSTRACT	18. NUMBER OF PAGES	19a. NAME OF RESPONSIBLE PERSON
a. REPORT	b. ABSTRACT	c. THIS PAGE			
unclassified	**unclassified**	**unclassified**	**UU**	**7**	

function of multiple frequencies contained in the UWB transmit pulse). The range dependence of their response may also differ from that of free-space targets.

As for any surface radar, interpretation of the detected signal must account for the effect of soil conductivity on RF propagation. The seminal theoretical work on such propagation was performed by Sommerfeld (Sommerfeld, 1909). A model of finite soil conductivity adequate for our purposes is implemented in the Numerical Electromagnetics Code (NEC) (Burke, 1977).

Our companion paper (Kohlberg et. al., 2008) describes an approach to computing the fully general target response, including the effects of the ground-air interface in both the near-field and far-field regimes. This analysis will be used to help determine the correct electrical circuit parameters for future experimental geometries and thereby help us further develop our detection and identification capability.

Targets taken in isolation are often well represented by a combined array of ideal, lossy, and/or reactive elements with non-ideal conductivity, permeability and permittivity. An analogy can be made to classic lumped parameter circuit modeling. A complex circuit can be represented by an appropriate combination of inductors, resistors, and capacitors (i.e., L, R, and C). Such simplified circuits of series and parallel connected elements have a complex but characterizable frequency response. The frequency response characteristics for different structures are unique enough to allow detection and classification of their returns.

3. MEASUREMENTS

Measurements are designed to establish proof-of-concept within a moderate budget. We use low-cost identical discone antennas as both transmitter and receiver. Each discone is equipped with a vertical whip to improve response at low frequency. Our transmitter power is relatively low; consequently, our target is entirely above ground for now.

Measurements are conducted at the Amtec Outdoor Test Range, on Bradford Drive in Huntsville, Alabama (Fig. 1).

Figure 1. Amtec Outdoor Test Range, Bradford Drive, Huntsville, AL. The measurement area is kept clear of equipment, vehicle, and personnel. Temporary shelters and coverings permit measurements to be made during adverse weather.

Figure 2 shows the experimental configuration in schematic form.

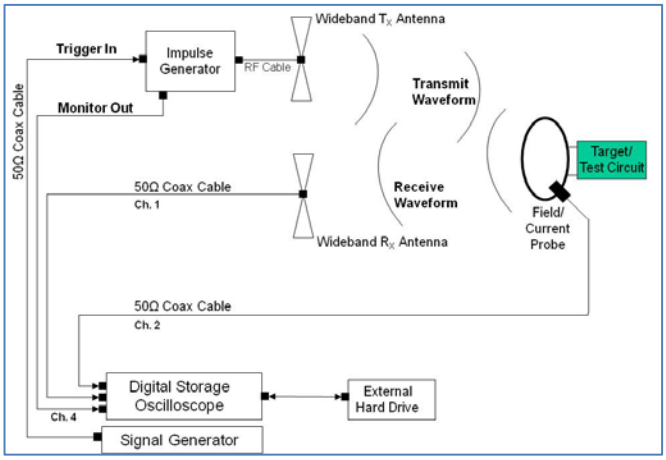

Figure 2. Experimental configuration. The signal generator (operated manually) initiates and synchronizes the procedure. The channel assignments--1, 2, and 4--correspond, respectively, to the yellow, blue, and green traces in Fig. 3. (Our sponsor has requested that we not provide equipment specifications.)

We excite the transmitter with a relatively low-amplitude one-kilovolt square pulse approximately five nanoseconds in duration. The transmitter response is shown (in green) in Fig. 3.

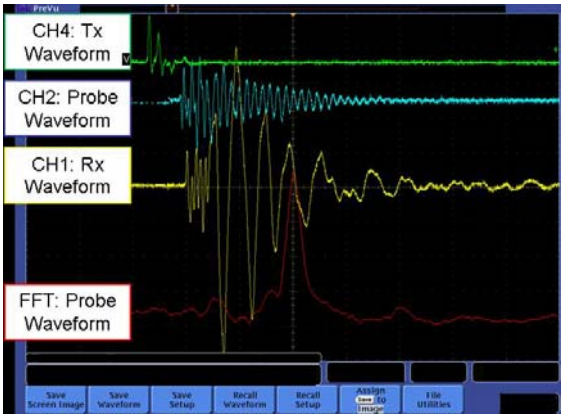

Figure 3. Time domain view of antenna and probe signals.

A ten-inch diameter copper loop (continuous except for a gap of approximately 1mm) served as a test circuit. The test circuit lies in the midplane between the two antennas. The loop axis is normal to the midplane, horizontal, and one meter above the ground. The loop is collocated with a small amount of clutter.

All of the waveforms are recorded and stored by a digital storage oscilloscope for later processing. Additionally, a current probe measures the test circuit excitation directly.

Measurement of the test circuit response is facilitated when the electromagnetic excitation of the target is spectrally as flat as possible. We approach this flatness in practice by applying a short voltage pulse (Fig. 3) to a transmitting antenna that is designed to have a flat response over the frequency range where we expect the strongest response (Fig. 4).

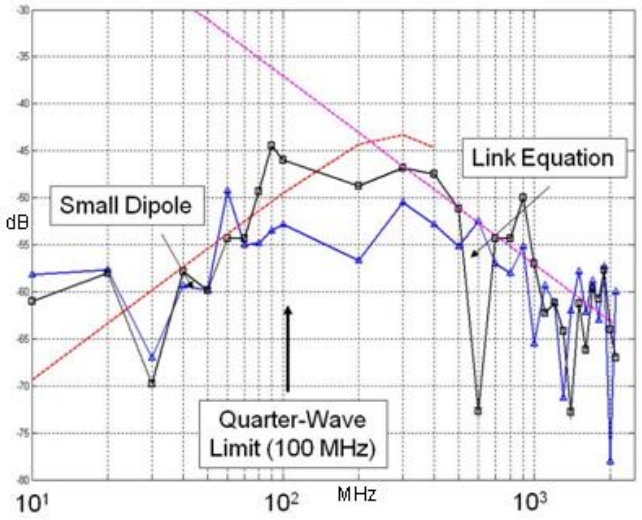

Figure 4. Discone antenna performance models in the low and high frequency limit [courtesy of Phase IV Systems].

For this paper, a series of measurements for the test circuit described were made at multiple ranges (Fig. 5).

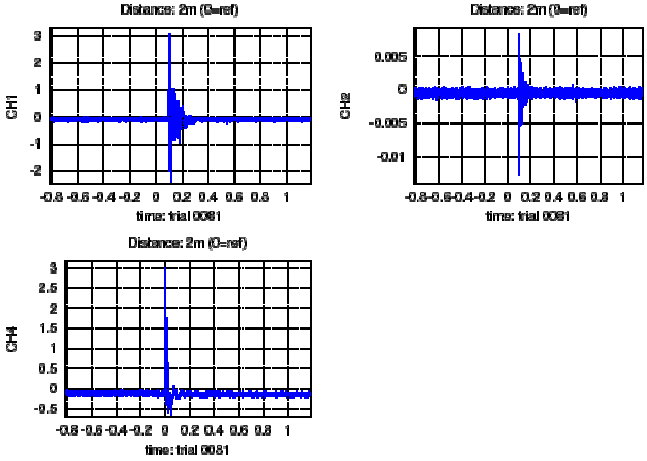

Figure 5. Receiver waveform (CH1), current loop waveform (CH2), and transmitter waveform (CH4) for a range of two meters. Similar data were recorded for range values of 5, 10, 25, 50, 75, and 100 meters.

Additionally, for each range, a series of measurements was made without the test circuit but with the test circuit supports in place. These latter (reference) measurements were made within a few minutes of the test circuit measurements. The reference measurements characterize the measurement system and background environment.

Identification and interpretation of the test circuit signature in the receiver waveforms is the subject of the next section.

4. DATA REDUCTION VIA PRINCIPAL COMPONENTS ANALYSIS

Principal components analysis (PCA) can be viewed as a means of data compression for analysis and classification. The approach taken here is as follows. Suppose that we obtain p sample waveforms $x_1(k), ..., x_n(k), ..., x_p(k)$, where k=1, ..., N is a discrete time index of each waveform $x_n(k)$ (taken to be a column vector) and where the same uniform time intervals apply for each waveform. For reasonably sized data sets, we may construct an N×p matrix $X = [x_1(k), ..., x_p(k)]$ containing all of the sample data. Let the matrix product

$$U\Sigma V^T = X \qquad (1)$$

be a singular value decomposition of X (Golub, 1996). The singular value decomposition expresses X as a product of two orthonormal matrices U and V, (i.e., $U^T U=I_p$, $V^T V=I_p$, where I_p is the appropriate identity matrix) and a diagonal matrix $\Sigma = diag(\sigma_1 \geq ... \geq \sigma_p)$. If we write U and V as arrays of length-N column vectors (i.e. $U=[u_1,...,u_p]$ and $V=[v_1,...,v_p]$), then we can also write

$$X = \sum_{n=1}^{p} \sigma_n u_n v_n^T, \qquad (2)$$

where u_n and v_n are unit vectors and $u_n v_n^T$ is a dyad. Note that the relative contribution of each $u_n v_n^T$ product is completely specified by the magnitude of the singular (scalar) value σ_n. Further, with the singular values sorted as above, the optimal two-norm rank-m approximation of X is

$$X_m = \sum_{n=1}^{m} \sigma_n u_n v_n^T, \qquad (3)$$

That is, we approximate the columns of X by linear combinations of the first m singular vectors $u_1,...,u_m$. In this sense, PCA can be viewed as the projection of the raw data into a low rank $\tilde{m}$-dimensional subspace. The relative magnitudes of the singular values σ_1, ..., σ_p provide a heuristic basis for the determination of the desired subspace dimension m.

We apply this simple PCA to the raw data collections described above. The data set contains p=460 sample waveforms. The original data waveforms have more than 10,000 samples, and a subset of N=2048 samples of the received pulse was used in the analysis. These windowed waveforms are what appear above in Fig. 5.

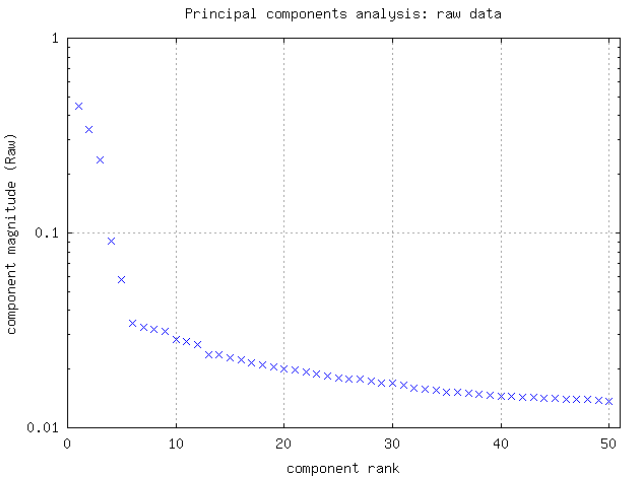

Figure 6. PCA of raw data: dominant singular values (N=2048, p=460).

The first 50 singular values of the resulting 2048×460 matrix X are shown in Fig. 6. Based on these values, the relevant data primarily occupies a five-dimensional subspace that is spanned by vectors u_1, u_2, u_3, u_4, u_5. Since these vectors are orthonormal, we can approximate each vector x_n, $n=1, \ldots, p$, as

$$x_n = \sum_{l=1}^{5} u_l (u_l^T, x_n), \qquad (4)$$

where the dot product (u_l^T, x_n) specifies the component of x_n in the u_l direction; i.e., how much does x_n "resemble" the feature u_l. The dot products (u_l^T, x_n) for $l=1, 2, 3, 4$ and each n value are shown at each target range in Fig. 7. (Note that each dot product is a sum over the time index k of the pairwise product of the kth elements of the two argument vectors.)

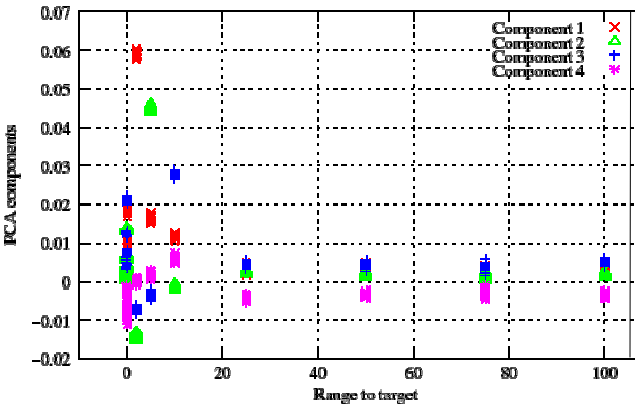

Figure 7: PCA of raw data: dot products of waveforms with the dominant basis vectors (the so-called principal components).

Observe that the PCA results are very consistent for the test circuit at ranges 2, 5, and 10 meters, and that the results at a range in excess of 20 meters are indistinguishable from one another. Nevertheless, the signatures for the test circuit at short range are remarkably consistent, which indicates that even this simple analysis can be used to establish the presence or absence of a target. The dominant four waveforms, u_1, …, u_4, are shown in Fig. 8 (next page).

From Fig. 7 we can see that the relative weightings of the principal components depend strongly on the range r, at least for $r \leq 20$ meters. This dependence permits us to use data correlation with various combinations of principal components as a range predictor. We (conservatively) use the first six principal components to

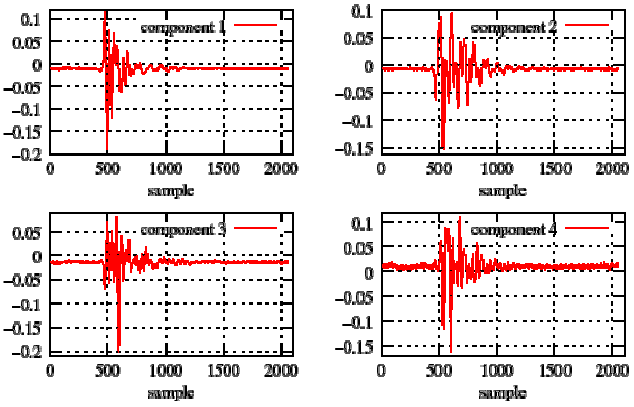

Figure 8. Raw-data principal components $u_1, \ldots, u_4$.

predict *1/r* when the test circuit is present or *0* for reference data. A least-squares data fit yields good results as seen in Fig. 9. Range to test circuit is reliably predicted for $r \leq 10$ meters. Beyond 10 meters our signal-to-noise ratio is too small to permit a reliable range prediction.

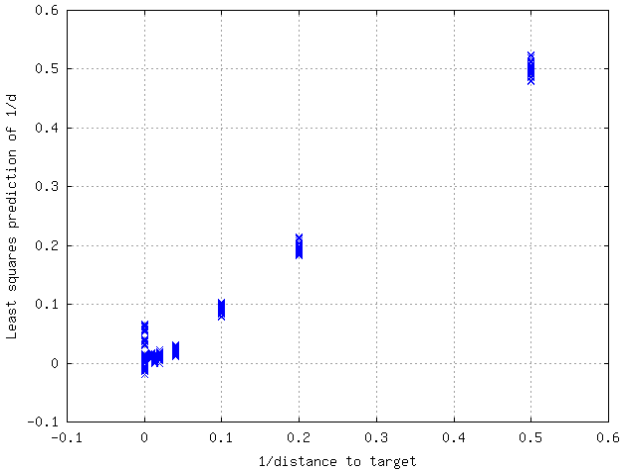

Figure 9. Raw PCA prediction of 1/r using the first 6 principal components. Prediction is reliable for $r \leq 10$ meters.

The PCA-data least-squares weights, means, and standard deviations for components 1 through 6 are given in Table I.

Table I. Principal Component Parameters.

Sorted PCA Index	Least Squares Weights	Mean Values of PCA Data	Standard Deviations of PCA Data
1	8.47497	1.2125e-02	0.0170924
2	0.89231	4.8627e-03	0.0150599
3	-1.13174	5.6242e-03	0.0095057
4	4.24965	-1.9782e-03	0.0037714
5	7.98134	1.8285e-04	0.0026825
6	-2.29150	-8.1767e-05	0.0016074

5. THEORETICAL PREDICTIONS

Numerical modeling of the experiment is accomplished with NEC (Numerical Electromagnetics Code, 1977). NEC computations are performed in the frequency domain and are based on the electric-field integral equation when modeling thin-wire structures, as is the case here. The electric-field integral equation is

$$\vec{E}(\vec{r}) = \frac{-i\eta}{k} \int_V \vec{\vec{G}}(\vec{r},\vec{r}') \cdot \vec{J}(\vec{r}')dV, \qquad (5)$$

where $\vec{\vec{G}}(\vec{r},\vec{r}') = (k^2\vec{\vec{I}} + \nabla\nabla)g(\vec{r},\vec{r}')$, $\vec{J}(\vec{r}')$ is the volume current distribution, k is the wavenumber (not to be confused with the time index of the previous section), $\omega\sqrt{\mu_0\varepsilon_0}$, $\eta = \sqrt{\mu_0/\varepsilon_0}$, ε_0 and μ_0 are, respectively, the free-space electric permittivity and magnetic permeability, $\vec{\vec{I}}$ is the identity dyad $\hat{x}\hat{x} + \hat{y}\hat{y} + \hat{z}\hat{z}$, and $g(\vec{r},\vec{r}')$, is the free-space scalar Green's function

$$g(\vec{r},\vec{r}') = \frac{e^{-ik|\vec{r}-\vec{r}'|}}{4\pi|\vec{r}-\vec{r}'|}. \qquad (6)$$

NEC includes a model for finite soil conductivity. The ground-air interface is, by convention, the z=0 plane.

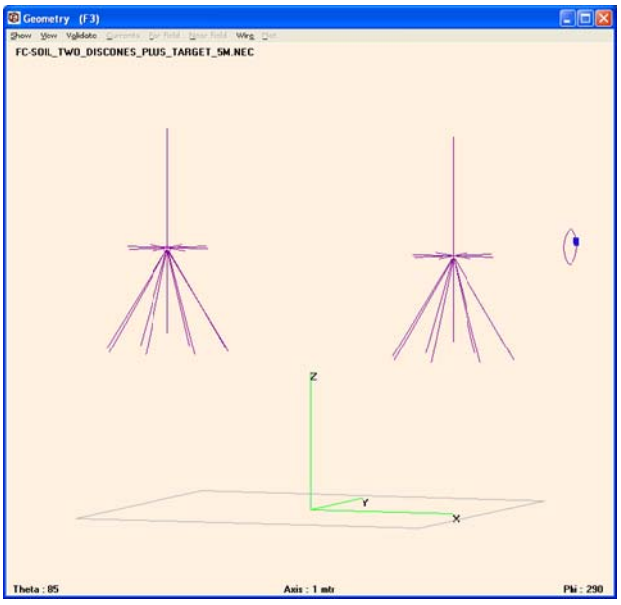

Figure 10. NEC model geometry. The target loop lies in the y-z plane. The y coordinate of the loop center is set to the range value for each computation

Figure 10 shows the components of our model. In the experiment the discones are supported by non-conductive posts; these support posts are not required in

the model. The loop is represented as a regular 16-gon. The dielectric properties of the gap between the ends of the loop are represented in the NEC model.

NEC provides an option to slowly sweep the frequency. We performed such a sweep using a ten-inch loop without the discone antennas. The result, which is insensitive to soil conductivity, is given in Fig. 11.

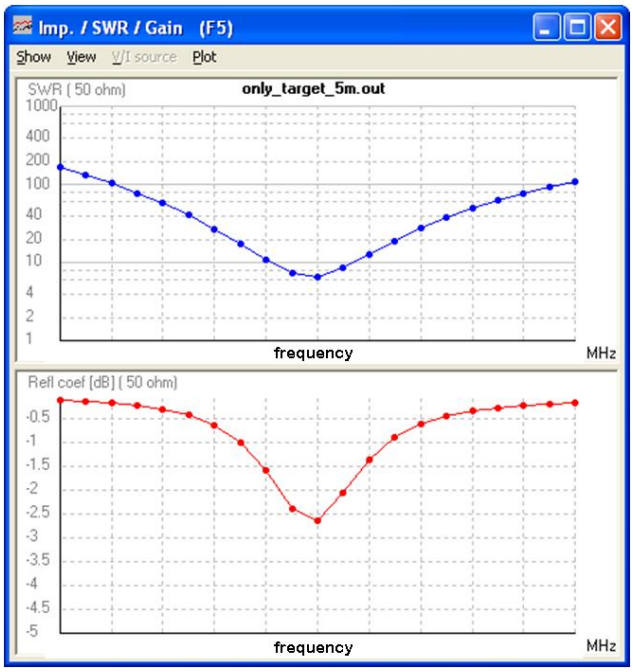

Figure 11. NEC frequency sweep of isolated wire loop. This result agrees with the spectrum of the measured target return and is insensitive to soil conductivity. (Note that we are not permitted to report detailed spectra.)

The test circuit response peaks at the dominant pole of the equivalent lumped parameter model. Subsequent NEC computations are performed at this frequency. Thus, the decay time ($\sim 1/\varsigma$) cannot be modeled by NEC directly. The decay time could, however, be inferred from the appropriate swept frequency computations.

To obtain the dominant test circuit response we perform two computations at each range. One computation models the propagation of radiation from the transmitter to the test circuit; the other models propagation from the test circuit to the receiver. The superposition principle and the absence of any nonlinear phenomena in our system guarantee that these computations may be performed independently and the results combined to obtain the full test circuit response (Fig. 12).

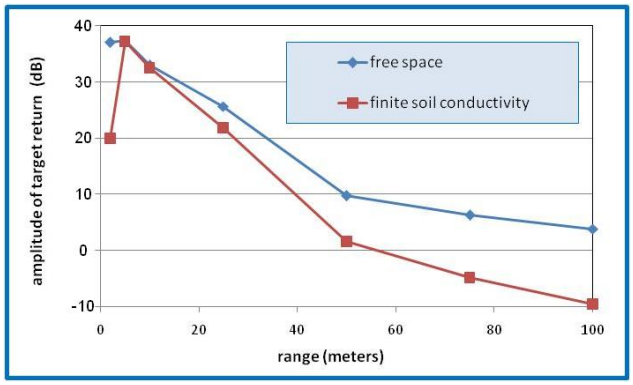

Figure 12. NEC-computed target-return amplitude (in arbitrary units) as a function of range for radiation at the dominant target mode frequency. The finite soil conductivity value is 0.007 mhos/meter.

The primary effect of finite soil conductivity is to attenuate the RF with respect to the purely free-space-propagation case. For our current geometry, this additional attenuation is about 3 dB for every 20 meters of range. We also expect that RF-ground coupling distorts the radiation pattern and, therefore, may impact the principal components that arise during the analysis of the experimental data. However, the PCA technique still applies.

6. ANALYSIS

A relatively simple principal component analysis can be used to establish the presence or absence of a test circuit. Additional PCA operations can predict the circuit range from the raw data. The inverse-range predictions shown in Fig. 9 involve the computation of dot products of the measured waveforms with the principal components dominant at each range. Consequently, they provide a measure of the test circuit response with much of the background removed.

These experimental results agree with NEC computations in that the test circuit is more easily detected at short range and that the induced response decreases rapidly with range.

For future measurements we plan to increase the amplitude of the voltage pulse delivered to the transmitter. This should increase the range of measurements with this particular test circuit and antenna configuration to between 20 and 40 meters, where soil conductivity plays a greater role.

CONCLUSIONS

Signatures have been observed and modeled for a target structure (a test circuit) in the field. A technique for reliably predicting range from the pulsed radar receiver signals is available, and the range dependence of the test circuit response can be inferred from these predictions. Theoretical predictions of test circuit response are consistent with these results. Test circuit response decreases rapidly with range.

NEC computations indicate that soil characteristics do play a role in test circuit response, and those computations are consistent with the test circuit response inferred from the range predictions.

During the next phase of our work we will apply this analysis and our measurement techniques to a wider variety of experimental geometries, including more complicated structures. Higher transmitter power should also be available. The same PCA technique used to predict range will be applied to target classification.

ACKNOWLEDGMENTS

We gratefully acknowledge the support of the U.S. Space and Missile Defense Command. We also appreciate technical assistance and advice provided by Steve Moren of Amtec Corporation, by Everett Farr of Farr Research, and by Jim Knaur and Dan Lawrence of Phase IV Systems, Inc.

REFERENCES

Baum, C.E., "Discrimination of buried targets via the singularity expansion**,"** *Inverse Problems,* **13,** pp. 557-570, 1997.

Burke, G.J. and Poggio, A.J., *"*Numerical Electromagnetics Code (NEC)--Method of Moments, Parts I & II: NEC program description–theory," Lawrence Livermore Laboratory, Livermore, CA, 1977 [content same as NOSC TD 116, Parts I & II].

Hanson, G. W., and Baum, C. E., "Perturbation formula for the natural frequencies of an object in the presence of a layered medium," *Electromagnetics,* 333–351, 1998.

Galagedara, L.W., Redman, J.D., Parkin, G.W., Annan, A.P., and Endres, A.L., "Numerical modeling of GPR to determine the direct ground wave sampling depth**,"** *Vadose Zone*, **J. 4**, pp. 1096-1106, 2005.

Golub, G.H., and Van Loan, C.F., *Matrix Computations*, Johns Hopkins University Press, 3rd edition, 1996.

Kind, T., Krause, I., and Maierhofer, C., **"**Development of a utility finding impulse radar**,"** *International Symposium on Non-Destructive Testing in Civil Engineering* (Berlin, Germany), September 16-19, 2003.

Kohlberg, I., S. von Laven, S.A., Albritton, N., McMillan, R., and Baginski, T., "Electromagnetic detection and identification of complex structures," Army Science Conference, Orlando, FL, December 1-4, 2008 (*accepted*).

Nag, S. and Peters, L., **"**Ramp response signatures of dielectric targets, especially landmines**,"** *Geoscience and Remote Sensing Symposium Proceedings*, **Vol. 1**, Issue, 6-10, pp. 213–215, July,1998.

Sommerfeld, A., "Über die Ausbreitlung der Wellen in der drahtlosen Telegraphie (Tr. Over the propagation of the waves in the wireless telegraphy)," *Annalen der Physik*, **Vol. 28**, pp. 665-736, March, 1909.

Venkatasubramanian, V., P. Liu, P., and Leung, H., "Chaos based UWB imaging radar for homeland security," *IEEE Conference on Cybernetics and Intelligent Systems*, **Vol. 1**, Issue, 1-3, pp. 351–355, 2004.